Chemical Engineering Journal 158 (2010) 505–512

Contents lists available at ScienceDirect

Chemical Engineering Journal

journal homepage: www.elsevier.com/locate/cej

Catalytic photodegradation of dyes by in situ zeolite-supported titania

Diego Ivan Petkowicz[a], Sibele B.C. Pergher[b,*], Carlos Daniel Silva da Silva[c], Zênis Novais da Rocha[c], João H.Z. dos Santos[a,**]

[a] Instituto de Química, Universidade Federal do Rio Grande do Sul (UFRGS), Av. Bento Gonçalves, 9500, Porto Alegre 91500-000, RS, Brazil
[b] Departamento de Química, Universidade Regional Integrada do Alto Uruguai e das Missões (URI), Campus Erechim, CP 743, Erechim 99700-000, Brazil
[c] Instituto de Química, UFBA, Campus de Ondina, Salvador 40170-290, Brazil

ARTICLE INFO

Article history:
Received 16 September 2009
Received in revised form 17 January 2010
Accepted 19 January 2010

Keywords:
Photocatalysis
Titania
Zeolite NaA
Dye
Rice husk

ABSTRACT

The degradation of dyes (methylene blue, direct blue 71, direct yellow 8) by a series of titania-supported catalysts generated in situ via the impregnation of $TiCl_4$ onto a series of zeolite, which was synthesized using rice husks as the silicon source, was individually evaluated. After calcination, the resulting supported catalysts were characterized by X-ray diffraction spectrometry, ultraviolet–visible diffuse reflectance spectroscopy, diffuse reflectance and transmittance infrared Fourier transform spectroscopy, energy dispersive X-ray scanning electron microscopy, small angle X-ray scattering and differential pulse voltammetry. The titania generated is present in the anatase phase, without affecting the zeolite framework. Catalyst activity was shown to be comparable to that of the commercial P-25 catalyst after 1 h of UV light exposition. Monitoring the catalyst performance of several batches of material showed that P-25 provided the highest photodecomposition until the third cycle. On the other hand, the activity of the in situ-supported titania catalyst, in spite of showing lower catalytic activity, remained roughly constant up to the fifth cycle. This suggests that the catalyst generated in situ is more suitable for both filtering and reuse.

1. Introduction

The disposal of industrial waste is a very relevant issue. Continuous research has been carried out to develop strategies for removing, destroying or recovering chemicals present in water. Dyes represent a serious danger for the aquatic environment. Several approaches have been employed for the treatment of waste water containing dyes, such as removal by biosorption [1], adsorption [2], electrocoagulation [3,4], ultracentrifugation [5] and photodecomposition [6,7]. The latter has been widely investigated, especially using titania as the catalyst.

The difficulties in recycling and preconcentrating restrict the usage of fine TiO_2 particles. Thus, TiO_2 has been supported on a number of inert materials for practical applications [8] including silica–clay composites [9], chitosan [10], bamboo charcoals [11], ceramic membranes [12], and as titania encapsulated composites [13]. Zeolites have also been proposed as hosts that can accommodate titania catalysts inside their pores [14]. Different kinds of zeolites have been explored, such as Y [15], Beta [16], ZSM-5 [17], mordenite [18] and MCM-41 [19,20].

In a previous study, we investigated zeolite synthesis employing alternative silicon sources, namely rice husk and chrysotile [21]. In the present study, we report the catalyst activity of the titania generated in situ from $TiCl_4$ impregnation on a zeolite support synthesized from rice husk, followed by calcination. The resulting potential photocatalysts were individually evaluated in the decomposition of some commercial dyes, namely direct blue 71 (DB), direct yellow 8 (DY) and methylene blue (MB). Scheme 1 depicts the structures of the dyes investigated.

Both commercial and synthesized NaA zeolites were employed in the preparation of the photocatalyst. For comparison, commercial P-25 was also used as a catalyst. The systems were characterized by a series of complementary techniques, namely: X-ray diffraction spectrometry (XRD), ultraviolet–visible diffuse reflectance spectroscopy (DRS), diffuse reflectance infrared Fourier transform spectroscopy (DRIFTS), transmittance Fourier transform infrared spectroscopy (FT-IR), energy dispersive X-ray scanning electron microscopy (SEM-EDX), small angle X-ray scattering (SAXS) and diffuse pulse voltammetry (DPV). Photodecomposition was monitored via UV–vis absorption spectroscopy.

* Corresponding author.
** Corresponding author. Tel.: +55 51 3308 7238; fax: +55 51 3308 7304.
E-mail addresses: pergher@uri.com.br (S.B.C. Pergher), jhzds@iq.ufrgs.br (J.H.Z. dos Santos).

1385-8947/$ – see front matter © 2010 Elsevier B.V. All rights reserved.
doi:10.1016/j.cej.2010.01.039

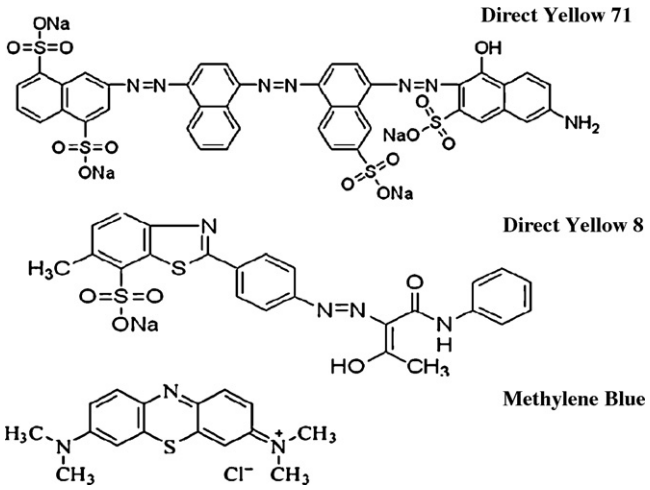

Scheme 1. Chemical structure of the investigated dyes.

2. Experimental

2.1. Materials

For the zeolite synthesis, the following reactants were used: sodium hydroxide (Quimex, P.A.), sodium aluminate (Aldrich, ≥99%) and distilled water (18 Ω). For comparison, a commercial zeolite NaA (Diatom Mineração Ltda, Mogi das Cruzes, Brazil) was also employed. Cationic exchange reactions were performed with calcium chloride (Fluka, ≥97%). Rice husk samples were provided by agricultural producers from Criciuma (Brazil). For the supported catalysts, titanium(IV)-chloride (Merck) and hexane (Merck) were used. P-25 was generously donated by Degussa. Methylene blue (Basic blue 9, Sigma–Aldrich), direct yellow 8 (Sigma–Aldrich), and direct blue 71 (Sigma–Aldrich) were selected as target dyes and were used as received.

2.2. Synthesis of zeolites and supported catalysts

Zeolites were synthesized as reported in detail elsewhere [21]. In a typical reaction, ca. 4 g of zeolite was added to 100 mL of a calcium chloride solution (1 mol L^{-1}) at 80 °C for 16 h. For the catalyst synthesis, 10 mL of a $TiCl_4$ solution in hexane (0.05 M) was poured onto ca. 0.1 g of zeolite. The slurry was stirred at 100 °C for 1 h. After solvent evaporation, the solid was dried at 110 °C and calcined in air at 400 °C for 4 h. The final loading of Ti was 10 wt.% Ti/zeolite. The titania-supported catalysts were labeled according to the origin of the zeolite support: NaA-Com-Ti 10% for the commercial zeolite, NaA-RH-Ti 10% for the zeolite produced using rice husk, and CaA-RH-Ti 10% for the zeolite synthesized using RH as the silicon source, followed by cationic exchange with calcium chloride.

2.3. Zeolites and catalyst characterization

Zeolites and supported titania catalysts were characterized via a series of complementary analytical techniques. Powder X-ray diffraction data were acquired on a Diffraktometer model D5000 (Siemens) using a Ni filter and CuKα (λ = 1.54 Å) radiation. Nitrogen adsorption analyses were measured on an automatic AUTOSORB-2 (Quantachrome) apparatus. Experiments were performed isothermally at −196 °C with samples (ca. 100 mg) that were dehydrated under vacuum at 300 °C for 3 h prior to measurement. The analytical data were processed using the BET equation for the surface area and by the Barrett–Joyner–Halenda (BJH) method for the pore size distribution.

Scanning electron microscopy was performed with a SEM SSZ 550 (Shimadzu) instrument. Diffuse reflectance infrared Fourier transform spectroscopy (DRIFTS) was carried out using an FT-IR spectrometer equipped with a diffuse reflectance attachment (Bomen). Analyses using the transmittance mode were measured using an FT-IR spectrometer with pressed KBr pellets, averaging 32 scans at 4 cm^{-1} resolution. Elemental analysis was carried out on a Noran Instruments EDX system connected to a JEOL JSM 6300F scanning electron microscope with an accelerating voltage of 20 kV. Samples were fixed on carbon tape on a stub and sputtered with gold before measurements. Diffuse reflectance spectra of titania-supported catalysts were obtained on a UV–vis spectrometer (Varian UV-cary-100), using an integration sphere accessory.

The SAXS experiments were carried out using synchrotron radiation at LNLS (Campinas, Brazil) with a wavelength λ = 1.488 nm. The beam was monochromatized by a silicon monochromator and collimated by a set of slits defining a pin-hole geometry. A solid-stated CCD detector (MAR 160) was used to collect two-dimensional (2D) images with 2048 × 2048 pixels located at 6752.5 mm of the sample. The q-range of the scattering curves was 0.02 $nm^{-1} \leq q \leq 0.49\ nm^{-1}$, where q is the scattering vector ($q = (4\pi/\lambda)\sin(\theta/2)$). The data were corrected for sample transmission and background scattering using an empty cell as reference. Samples were placed in stainless steel sample holders closed by two mica windows.

Differential pulse voltammetry (DPV) measurements were conducted on a potentiostat/galvanostat (PARC, model 273). All experiments were carried out using a conventional three electrode cell. The titania electrode (S = 0.152 cm^2) and glassy carbon (0.082 cm^2) were used as the working electrode. The working titania electrode consisted of a PVC body containing a graphite disk, which supported the carbon past. Carbon past was prepared by mixing high purity graphite (Fisher Scientific) and the titania materials in a 9:1.5 (w/w) ratio with a few drops of oil. Ag/AgCl was used as the reference electrode and platinum wire as the auxiliary electrode. All measurements were carried out under high purity argon. $NaBF_4$ solutions were employed as supporting electrolyte.

2.4. Photocatalytic reaction

The resulting catalysts were evaluated in the photodecomposition of dyes using UV irradiation from a medium pressure 250 W Hg lamp (λ_{max} = 365 nm). The decomposition reaction was carried out in a quartz reactor equipped with a cold finger. In a typical reaction, ca. 0.05 g of catalyst (or 0.008 g pure P-25) and 150 mL of a dye solution (30 mg L^{-1}) were stirred and irradiated for 1 h. Aliquots were collected after the 1 h irradiation and the remaining dye concentration was monitored by UV–vis spectroscopy (Shimadzu UV-160A) by measuring the centrifuged solution at different wavelengths, according to their electronic spectra, as depicted in Fig. 1.

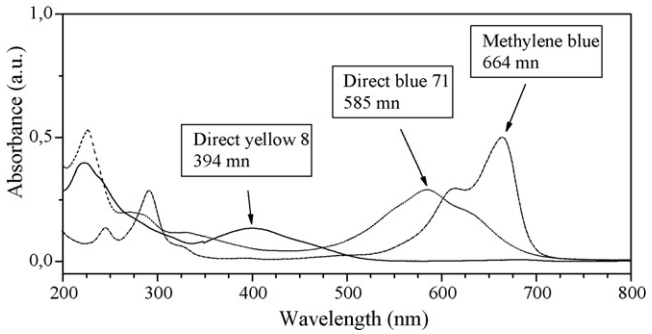

Fig. 1. Electronic spectral of the photodecomposition of dyes.

Table 1
Equation's parameters of the calibration curves ($N = 7$) and wavelength employed in the measurement.

Dyes	R	Equation	λ (nm)
Methylene blue	0.9989	$Y = 0.00495 + 0.09372X$	291
Direct blue 71	0.9999	$Y = 0.01280 + 0.02879X$	585
Direct yellow 8	0.9995	$Y = 0.00102 + 0.01332X$	394

The dye concentration was determined via the calibration method individually developed for each dye, as shown in Table 1.

In the case of the real sample, surface water samples were collected from a stream located in Porto Alegre, Brazil (30°06′52.46″S; 51°06′22.75″N). The samples were initially passed through a filter of porosity 0.45 μm, and further spiked with a known concentration of dye (30 mg L^{-1}).

3. Results and discussion

Fig. 2 shows the X-ray diffraction patterns of the synthesized zeolites, using commercial silica (a) and the different titania-supported catalysts (b–d). For comparison, the diffractogram of commercial P-25 titania (e) is also included.

According to Fig. 2, with the exception of CaA-RH-Ti 10%, the characteristic XRD peaks of anatase phase could be observed at $2\theta = 25.4°$, 48.3° and 54.9°, and were independent of the support used. No signals corresponding to the rutile phase ($2\theta = 27.4°$) could be detected [22]. Furthermore, for CaA-RH-Ti 10%, peaks corresponding to the anatase or even the rutile phases were not detected, thereby suggesting that amorphous TiO_2 might be formed in this system. Such behavior could be due to the larger opening of the pores, resulting from the cationic exchange.

The supported catalysts were further characterized by infrared spectroscopy. By transmission mode analysis, all materials showed characteristic vibrations assigned to the zeolite structure [23]. No band at ca. 960 cm^{-1} was observed for any of the three supported catalysts, suggesting that the substitution of Ti into tetrahedral Si sites during calcinations process did not take place. Therefore, it is very likely that there is no chemical bonding between the generated TiO_2 moieties and the zeolite framework. Titania domains might be created on the zeolite surface or could be partly encapsulated into the zeolite cavities [24–26].

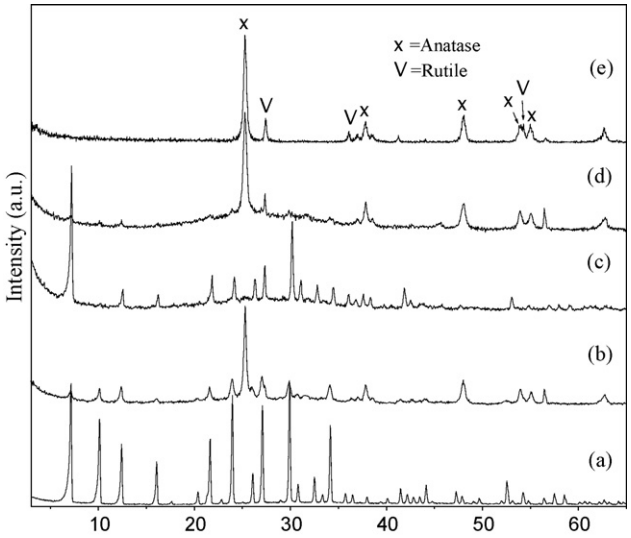

Fig. 2. X-ray diffractogram of the (a) NaA-RH, (b) NaA-Com-Ti 10%, (c) CaA-RH-Ti 10%, (d) NaA-RH-Ti 10% and (e) P-25.

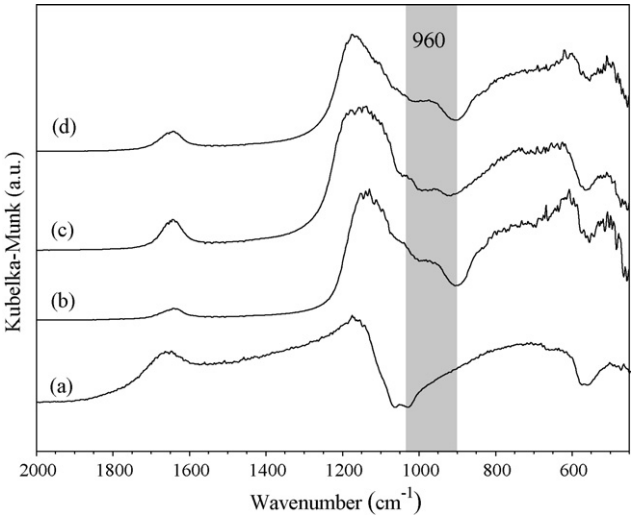

Fig. 3. FT-IR spectrum of: (a) NaA-RH, (b) NaA-Com-Ti 10%, (c) NaA-RH-Ti 10% and (d) CaA-RH-Ti 10%.

Fig. 3 shows diffuse infrared reflectance spectra (DRIFTS) of these systems.

According to Fig. 3, all catalysts showed a band shoulder at ca. 960 cm^{-1}, which was assigned to the antisymmetric stretching vibration of Ti–O–Si bonds. This suggests that Ti–O–Si moieties might be present on the external surface [24,25] since DRIFTS is more sensitive for signals from the uppermost surfaces, whereas transmittance FT-IR detects signals coming from both the bulk and surface of the sample.

Fig. 4 shows the DRS spectra in the UV–vis region for the different supported systems. The absorption band at ca. 200–260 nm is due to electron transfer excitation from the ligand-oxygen to an unoccupied orbital of the Ti^{4+} framework [27–29]. The spectra are also characterized by a large band centered at 350 nm, which is assigned to the electronic transition from 2p(O) to 3d(Ti), corresponding to the valence band to the conduction band transition according to the energy band structure of TiO_2 [22].

The diffuse reflectance spectra in Fig. 4 show one weak absorption band with a maximum at ca. 210 nm, attributed to the tetracoordinated titanium. The shoulder observed at ca. 350 nm is characteristic of the titanium dioxide outside of the framework. A broader shoulder at ca. 280 nm, present in the CaA-RH-Ti 10% sample, indicates the presence of partially polymerized hexacoor-

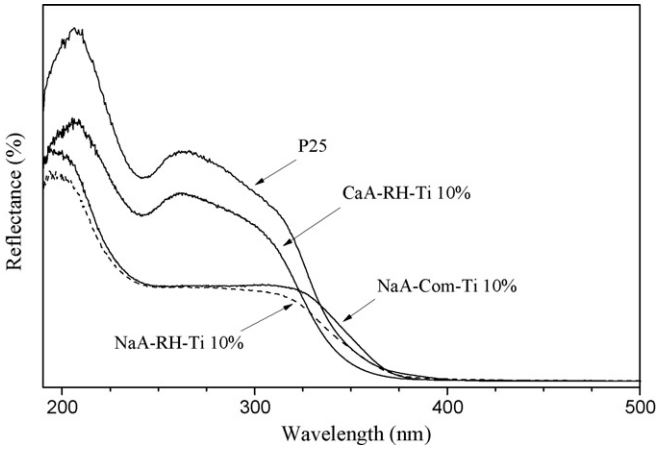

Fig. 4. Diffuse reflectance spectra of the titania supported zeolites obtained from different silicon sources.

Table 2
Band gap and absorption values for the titania-systems.

Material	Band gap (eV)	Absorption threshold (nm)
P-25	3.20	385
NaA-Com-Ti 10%	3.31	375
NaA-RH-Ti 10%	3.36	369
CaA-RH-Ti 10%	3.55	349

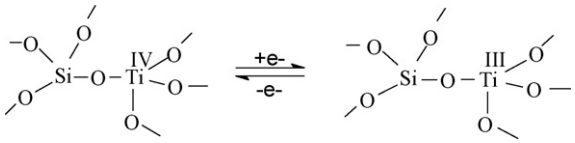

Scheme 2. Reduction of Ti(IV) in zeolite–titania.

dinated Ti species containing Ti–O–Ti moieties [30,31], which is similar to the band observed in the spectrum of P-25.

The determination of the band gap from the UV–vis spectra is an alternative method to study the modification of the electronic properties of the TiO_2 species [31,32]. Band gap and absorption thresholds were calculated using the UV–vis reflectance spectra according to the literature [22].

Despite the different slopes associated to the electronic transition bands presented in Fig. 4, the results shown in Table 2 indicate that there are no significant differences in the band gaps, except for in CaA-RH in which the value was relatively high (3.55 eV). This result may be due to the low crystallinity of titania detected in this sample, as previously shown in Fig. 2. It is worth noting that such values are relatively higher than to those recently reported for nanocrystalline mesoporous-assembled TiO_2, synthesized by sol–gel process [33], suggesting that the obtained catalyst may be richer in anatase phase.

The Ti distribution along the zeolite grain was further monitored by SEM-EDX by measuring the atomic concentration at 20 spots. Metal distribution is relatively homogeneous: $Ti/Si = 0.655 \pm 0.167$ for CaA-RH and 0.997 ± 0.526 for NaA-RH-Ti 10%, taking into account that the standard deviation is very small. It is worth noting that a higher bias was observed for the catalyst NaA-RH-Ti 10%. This behavior could be attributed to lower pore diameter present in the zeolite (4 Å), which might make incorporation of the solvent (cyclohexane) more difficult and might promote titania cluster formation on the zeolite crystal surface. Such a configuration might cause a lower homogeneity in the Ti distribution. SEM analyses suggest the presence of such agglomerates as shown in the micrographics in Fig. 5.

Fig. 5 shows the SEM micrographics of the zeolites, titania supported zeolites and of P-25. The micrographics a–f exhibit coffin-like cubic crystals, which are typical of a LTA-type zeolite, with a primary particle size of ca. 1 μM. It is worth noting that micrometer sized particles allow easier filtration procedures, and therefore reuse, in contrast to the P-25 nanometer-sized particles (Fig. 5g), which are harder to recover. Furthermore, according to Fig. 5, the crystal size remains roughly constant after the Ti impregnation.

Table 3 presents the results of surface area calculated by the BET method, for the zeolite NaA, before and after impregnation of the $TiCl_4$.

Relatively low surface area values are observed in Table 3, which is consistent with the data expected for the zeolite NaA. Ionic exchange attempts were carried out using $CaCl_2$ (0.1 mol L^{-1}) solutions at 80 °C for 16 h. The resulting materials were further analyzed by nitrogen adsorption. According to Table 3, after cationic exchange with Ca^{2+} (CaA-RH), the surface area increased from 6.3 to 486 $m^2\,g^{-1}$. Nevertheless, after impregnation of the $TiCl_4$, a reduction is observed, probably due to the TiO_2 cluster formation within the pores. In the cases of NaA-Com and NaA-RH there was not a significant variation in surface area was detected.

Fig. 6 shows the profiles of differential pulse voltammograms (DPV) obtained with carbon paste electrodes modified with the titania–zeolite catalysts in aqueous solution. In the voltammograms, one cathodic peak at −1600 mV for NaA-RH-Ti 10% (curve a) is observed, and a second peak is also observed at ca. −1400 mV vs. Ag/AgCl for CaA-RH-Ti 10% (curve b). In the former, an additional cathodic wave was observed at −1000 mV with a shoulder around −650 mV vs. Ag/AgCl (cathodic scan). These waves at negative potential are detected with values similar to that of TiO_2 (P-25) [23]. This behavior is in agreement with TiO_2 in zeotype matrices [32].

According to the literature, the PDV of P-25 has shown a pair of peaks at +510 vs. Ag/AgCl [23], attributed to the redox process $Ti^{4+/3+}$ (Scheme 2). The UV–vis reflectance spectra suggest that different types of titanium could also be present in P-25. The energy of the bands seems to correspond to tetrahedral and octahedral coordinated Ti. The absence of waves for titanium-zeotypes is probably due to structural differences (Fig. 6).

In the DPV of the systems shown in Fig. 6, the observed shoulders around −500 mV (curve b) and −700 mV (curve a) in titanium-zeotypes, in analogy to nanocrystalline film of titania [32], could be assigned to Ti^{3+} generated on the surface of titania. At more negative potentials, the DPV for NaA-RH-Ti 10% zeotype shows a wave at −1000 mV and another one at −1500 mV. These results are also similar to those reported for the nanocrystalline titania film, in which spectroelectrochemical changes were assigned to the reduction of the Ti^{4+} to Ti^{3+}. The absence of a cathodic wave at −1000 mV in CaA-RH-Ti 10% zeotype is consistent with structural differences for titanium-zeotypes, showed previously in Fig. 2c. In addition, the intensity and wave profile of these cathodic peaks are dependent upon the pH (not showed). Thus, the degree of reduction of $Ti^{4+/3+}$ on the surface changes with the pH.

Fig. 7 shows the percentage of dye decomposition by the in situ-supported titania–zeolite and P-25, in the presence of UV irradiation.

According to Fig. 7, the nature of the supported catalyst affects the extent of decomposition of the evaluated organic dyes. It is worth noting that P-25 exhibited the highest catalyst activity. Among the prepared supported catalysts, the NaA-based catalysts showed roughly comparable activities. On the other hand, CaA-RH had low photocatalytic activity, possibly due to the absence of the anatase phase, as previously shown in Fig. 2.

Table 3
Surface area of zeolite NaA, before and after impregnation of the $TiCl_4$.

Sample	Surface area ($m^2\,g^{-1}$)[a]	
	Before impregnation	After impregnation
NaA-Com	6.2	6.6
NaA-RH	6.3	6.8
CaA-RH	486	50

[a] ±10%.

Table 4
Surface fractal dimension (D_s) of zeolite and supported titania catalysts.

Catalyst	q-range (nm^{-1})	D_s	Band gap (eV)
P-25	0.1–0.4	2.2	3.2
Zeolites		2.2	–
CaA-RH-Ti 10%		2.4	3.55
NaA-RH-Ti 10%		2.6	3.36
NaA-Com-Ti 10%		2.8	3.31

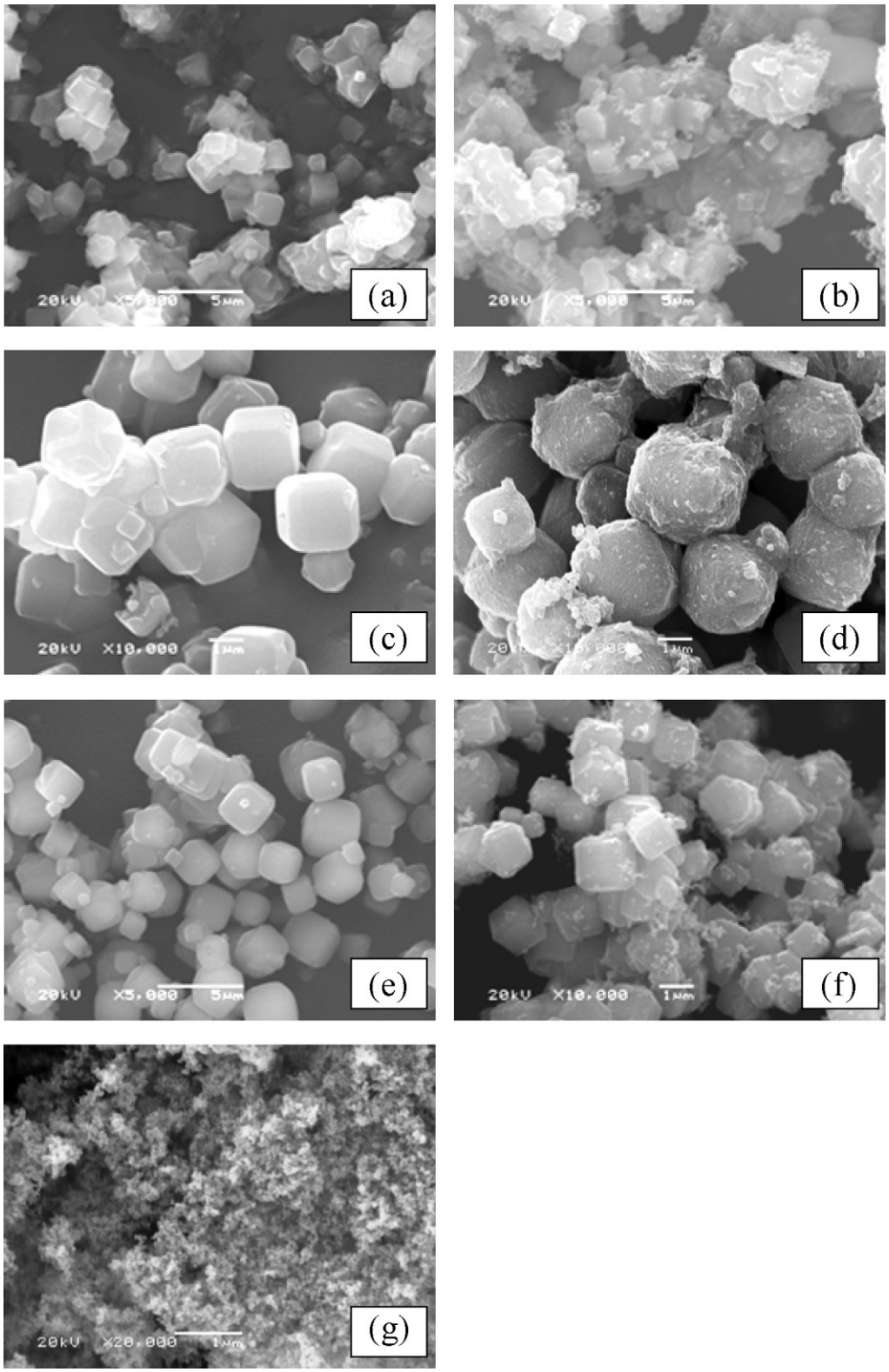

Fig. 5. Micrographs of: (a) NaA-Com, (b) NaA-Com-Ti 10%, (c) CaA-RH, (d) CaA-RH-Ti 10%, (e) NaA-RH, (f) NaA-RH-Ti 10% and (g) P-25.

The catalyst systems were further characterized by SAXS. Table 4 shows the values of surface fractal dimension of the resulting photocatalyst. For comparative reasons, data from commercial P-25 and the zeolites were also included.

According to Table 4, the values of surface fractal dimension of all catalyst are larger than 2. This suggests that the secondary particles of the samples have a rough pore–solid interface with dense core [34].

According to Table 4, after titania impregnation on the zeolite surface, there was an increase in the surface fractal dimension (D_S) in comparison to the zeolite before the impregnation ($D_S = 2.2$, for all the prepared zeolites). For the resulting photocatalyst systems,

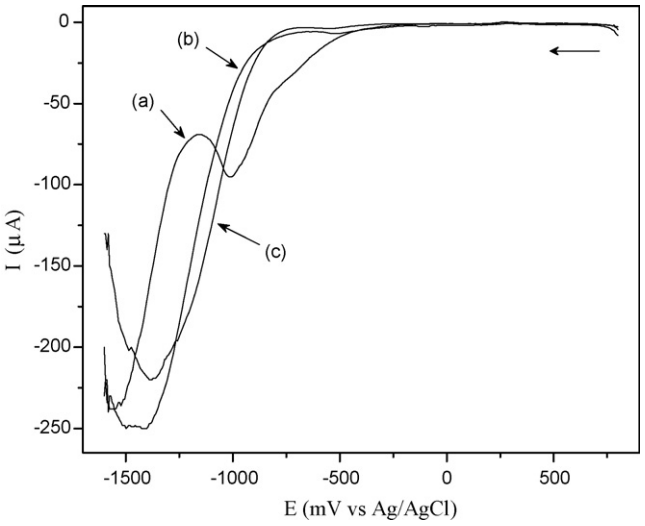

Fig. 6. Differential pulse voltammograms of: (a) NaA-RH-Ti 10%, (b) CaA-RH-Ti 10% and (c) CaA-RH. Aqueous solution pH = 1. Scan rate (υ) = 25 mV s^{-1}.

different D_s values were observed, which in turn, seemed to be related to the photocatalyst activity: the bigger the D_s value, the higher the catalyst activity. This behavior can be assigned either to an increasing in the contact area, or to a reduction in the band energy gap. Comparing data from Table 4 with those in Fig. 7, the following trend can be extracted in terms of photocatalyst activity: P-25 > NaA-Com-Ti 10% > NaA-RH-Ti 10% > CaA-RH-Ti 10%, in which NaA-Com-Ti 10% exhibited the highest activity among the supported catalysts.

The DPV profile of DB was analyzed both before and after the photolysis. DB voltammograms in aqueous medium (pH = 5), in which an anodic peak and corresponding cathodic peak around +50 mV, as well as another anodic peak in range of +200 to +660 mV vs. Ag/AgCl are detected with graphite-P-25 as the working electrode, before and after UV irradiation, in an argon and oxygen atmosphere. In an oxygen atmosphere, the peak at +50 mV is shifted to a lower positive potential (around +2 mV) and the current intensity decreased after irradiation. For the studies under an argon atmosphere, an increase of the current intensity was observed in the anodic peak around +50 mV and in the other peaks at more positive potentials.

In the literature, the photocatalytic activity of titania on the degradation of DB by UV irradiation was reported [35], by monitoring the decrease of the absorption band centered at 584 nm. In analogy to the reported data, and taking into account the present study, one can infer that the alteration in the PDV profile for DB can be due to the photodegradation of the dye on the electrode surface. Similar behavior was observed for the other titania–zeolite based catalysts, but the profile in DPV is more complex.

DB is a triazo compound with a π–π conjugated systems and its electrochemical polymerization on the vitreous carbon electrode surface has been already reported [36]. In the present study, we have investigated the PDV profiles for DB before and after irradiation on the graphite electrode surface modified with titania. As shown in Fig. 9, the four anodic peaks on the PDV profiles can be attributed to the polymerization process of the dye on the vitreous carbon electrode [36]. This process leads to the formation of species that are more easily oxidized as a dimer, trimer, tetramer and ultimately, a polymer. The presence of several anodic peaks in PDV indicates coupling reaction after oxidation of primary amino groups in DB. After UV–vis irradiation, a change in the current intensity was observed suggesting that the detected peaks might be due to photopolymerization. This behavior was observed in both argon and oxygen atmospheres, as in the case of the titania electrode (NaA-Com-Ti (10%) Fig. 8) and of NaA-RH-Ti 10%. In the presence of the titania supported system, the current intensity of the anodic peaks at less positive potential and around +200 mV was higher as compared in the case of only UV irradiation. This result can be attributed to the catalytic efficiency of titania supported on a NaA zeolite.

Despite the fact that the pulse voltammograms measured in the systems after irradiation under oxygen or argon atmospheres show current alterations, which are a fundamental basis of the role of TiO_2 at the different materials, the same relationship is not observed from the catalytic point of view. The higher catalyst efficiency observed for CaA-RH-Ti 10% in the decomposition of DY under an oxidizing atmosphere, if compared under an argon atmosphere, can be a consequence of electron transfer from the conduction band (eCB^-) for the adsorbed O_2 on the photocatalyst (Eq. (1)), which results in the generation of superoxide radical ($O_2^{\bullet -}$). Such species would be responsible for the photodegradation of dyes, as represented in Eqs. (1)–(6). Since the experiments were carried out in aqueous medium, the formed $O_2^{\bullet -}$ radical (Eq. (1)) reacts with H^+(aq) and results in the hydroxyperoxyl ($HO_2^{\bullet}$) radical (Eq. (3)), which is converted into H_2O_2, an oxidizing agent which received an electron from the conduction band (eCB^-) (Eqs. (3) and (4)) and results into the hydroxyl radical ($OH^{\bullet}$). The latter is

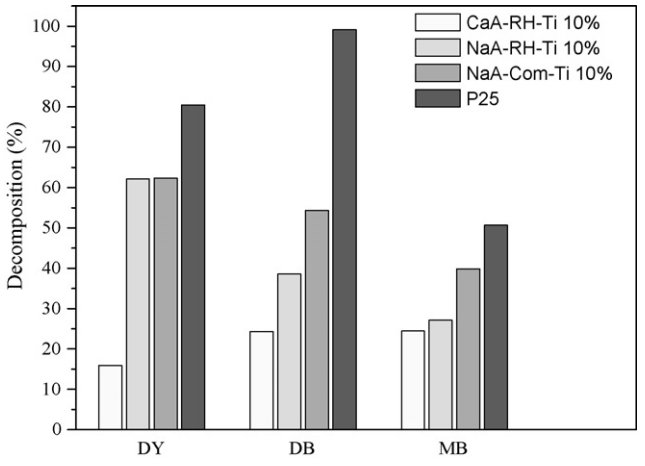

Fig. 7. Percentage of the decomposition of dyes by in situ-supported titania–zeolite and P-25, after 1 h of UV irradiation.

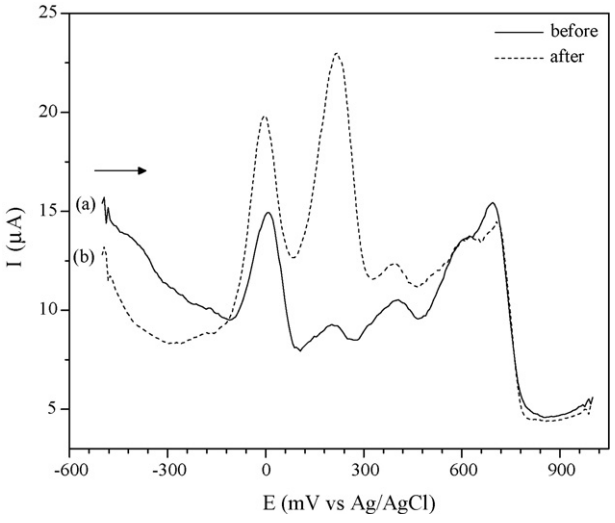

Fig. 8. Differential pulse voltammograms with anodic scan of DB in aqueous solution pH = 5 and υ = 100 mV s^{-1}. Working electrode: graphite-NaA-Com-Ti 10% before and after UV irradiation in argon atmosphere (15 min).

a strong oxidizing agent, and therefore promotes the degradation of DY, as well as of the other evaluated dyes (Eq. (5)):

$$O^{\bullet -}_{2(\text{adsorbed titanium-zeotypes})} + eCB^{-} \rightarrow O_2{}^{\bullet -} \quad (1)$$

$$O_2{}^{\bullet -} + H^{+} \rightarrow HO_2{}^{\bullet} \quad (2)$$

$$2HO_2{}^{\bullet} \rightarrow H_2O_2 + O_2 \quad (3)$$

$$H_2O_2 + eCB^{-} \rightarrow OH^{\bullet} + OH^{-} \quad (4)$$

$$\text{dye} + OH^{\bullet} \rightarrow \text{degradation of dye} \quad (5)$$

Furthermore, the potential of the generated electron–hole pair in the valence band (hVB^{+}) is positive enough to oxidize the dye molecules (Eq. (6)), and the conduction band electron (eCB^{-}) is negative enough to reduce the dye molecules (Eq. (7)):

$$\text{dye} + hVB^{+} \rightarrow \text{oxidation of dye} \quad (6)$$

$$\text{dye} + eCB^{-} \rightarrow \text{reduction of dye} \quad (7)$$

Thus, considering the previous discussion on the electrochemical behavior of these catalysts under argon or oxygen atmospheres, it seems that there is a divergence between the studies carried on through the alteration of the DPV profile and the photocatalytic studies involving NaA-Com Ti (10%) and P-25. Nevertheless, it is worth noting that the former depicts the formation of the photodegraded product on the electrode surface, while in the latter, the products generated in solution are evaluated.

The oxidative degradation of the evaluated dyes seems to involve the reaction between adsorbed O_2 onto the titania-based zeolite particles, which is transformed into hydroxyl radical ($OH^{\bullet}$) by UV radiation. These radicals, in turn, lead to the production of different products. By means of DPV experiments, it is possible to suggest that the charge transfer mechanism between hVB^{+} and the dye is an important step during the process.

The efficiency of the photocatalysts was further analyzed with a real sample (surface water) collected in a stream. The sample was spiked with a known concentration of the DY (30 mg L^{-1}). For comparison, the results previously obtained for the photodegradation of DY were included in Fig. 9.

According to Fig. 9, the catalyst activity was shown to be lower for the stream water sample for all catalyst systems. This observed effect may be due to the fact that natural water may contain inorganic substance, such as phosphates, sulfates, chlorides, carbonates and nitrates, which are capable of being absorbed on the TiO_2 surface [37]. Furthermore, the presence of humic acid may also cause a negative effect by consuming the hydroxyl radical [38].

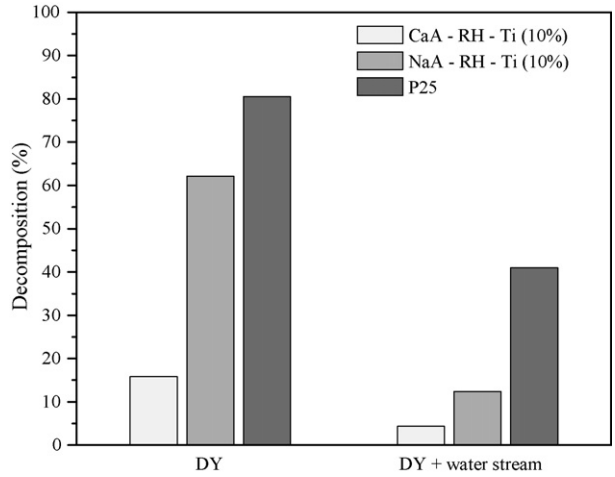

Fig. 9. Photodegradation of the water stream spiked with a known concentration of the DY (30 mg L^{-1}). Time of UV irradiation: 1 h.

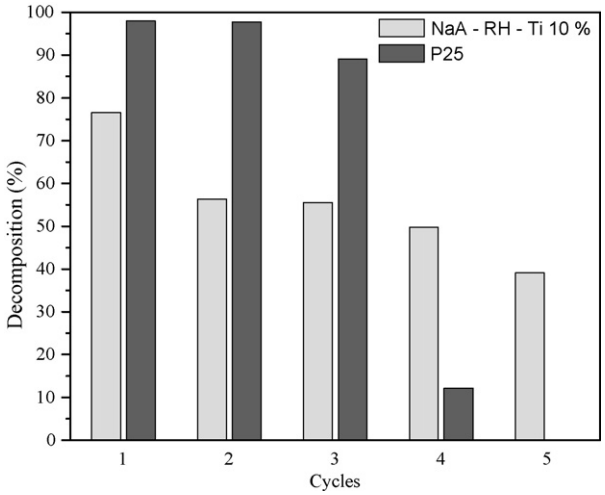

Fig. 10. Photodegradation cycles of the DY for NaA-RH-Ti 10% and P-25, after 1 h of irradiation.

Fig. 10 shows the performance of NaA-RH-Ti 10% and P-25 photocatalysts in the degradation of DY after five runs. For these experiments, after 1 h of irradiation, the catalyst was separated from the solution by filtering and drying at 110 °C for 4 h. The solid was reused in a new experiment. This procedure was repeated for an additional four cycles.

According to Fig. 10, P-25 initially exhibited the highest photodecomposition activity up to the third cycle, but thereafter, it declined abruptly, and no activity was observed in the fifth one. On the other hand, the NaA-RH-Ti 10%, in spite of showing lower catalyst activity, remained roughly constant up to the fifth cycle.

4. Final remarks

Zeolite-supported titania catalysts, prepared via the impregnation of $TiCl_4$, are a simple means to produce active photocatalysts, which can be synthesized from alternative materials like rice husks. The advantage of such supported catalysts, in comparison to commercial titania, principally resides in their grain size, which makes them easier to separate and to reuse. The present supported catalyst size is in the micrometer range, while the commercial one is in the nanometer range. Zeolite NaA was shown to act as an inert support, which did not affect the titania band gap. The differential pulse voltammetry for dye on graphite electrode surface modified with titania supported on zeolite, shows that the higher activity of the UV process may be due to the electron transfer between eCB^{-} or hVB^{+} in TiO_2 and dye. Nevertheless, one cannot neglect the possibility that the sorptive characteristics of such zeolitic materials might partly contribute to the adsorption of the dye to be reduced, affording a high degree of photodecomposition under UV irradiation. The catalyst activity of NaA-RH-Ti 10%, also remained roughly constant through several cycles.

Acknowledgements

This project was partially financed by CNPq. D.I. Petkowicz thanks CAPES for the grant. We are grateful to Degussa for their donation of P-25. The authors thank LNLS for measurements on the SAXS (Project SAXSS1-5296) beamline.

References

[1] F. Çolak, N. Atar, A. Olgun, Biosorption of acidic dyes from aqueous solution by *Paenibacillus macerans*: kinetic, thermodynamic and equilibrium studies, Chem. Eng. J. 150 (2009) 122–130.

[2] G. Bayramoglu, B. Altintas, M.Y. Arica, Adsorption kinetics and thermodynamic parameters of cationic dyes from aqueous solutions by using a new strong cation-exchange resin, Chem. Eng. J. 152 (2009) 339–346.
[3] B. Merzouk, B. Gourich, A. Sekki, K. Madani, Ch. Vial, M. Barkaoui, Studies on the decolorization of textile dye wastewater by continuous electrocoagulation process, Chem. Eng. J. 149 (2009) 207–214.
[4] M. Eyvaz, M. Kirlaroglu, T.S. Aktas, E. Yuksel, The effects of alternating current electrocoagulation on dye removal from aqueous solutions, Chem. Eng. J. 153 (2009) 16–22.
[5] A.L. Ahmad, S.W. Puasa, Reactive dyes decolourization from an aqueous solution by combined coagulation/micellar-enhanced ultrafiltration process, Chem. Eng. J. 132 (2007) 257–265.
[6] J. Saien, M. Asgari, A.R. Soleymani, N. Taghavinia, Photocatalytic decomposition of direct red 16 and kinetics analysis in a conic body packed bed reactor with nanostructure titania coated Raschig rings, Chem. Eng. J. 151 (2009) 295–301.
[7] C.-C. Mao, H.-S. Weng, Promoting effect of adding carbon black to TiO_2 for aqueous photocatalytic degradation of methyl orange, Chem. Eng. J. 155 (2009) 744–749.
[8] Y. Xu, C.H. Langford, Photoactivity of titanium dioxide supported on MCM41, zeolite X and zeolite Y, J. Phys. Chem. B 101 (1997) 3115–3121.
[9] F. Li, Y. Jiang, M. Xiaa, M. Suna, B. Xuea, X. Ren, A high-stability silica–clay composite: synthesis, characterization and combination with TiO_2 as a novel photocatalyst for Azo dye, J. Hazard. Mater. 165 (2009) 1219–1223.
[10] Z. Zainal, L.K. Hui, M.Z. Hussein, A.H. Abdullah, I.R. Hamadneh, Characterization of TiO_2 chitosan/glass photocatalyst for the removal of a monoazo dye via photodegradation adsorption process, J. Hazard. Mater. 164 (2009) 138–145.
[11] C.H. Wu, J.F. Shr, C.F. Wu, C.T. Hsieh, Synthesis and photocatalytic characterization of titania supported bamboo charcoals by using sol–gel method, J. Mater. Process. Technol. 203 (2008) 326–332.
[12] Y.H. Wang, X.Q. Liu, G.Y. Meng, Preparation and properties of supported 100% titania ceramic membranes, Mater. Res. Bull. 43 (2008) 1480–1491.
[13] R. Venkatasubramanian, R.S. Srivastava, R.D.K. Misra, Comparative study of antimicrobial and photocatalytic activity in titania encapsulated composite nanoparticles with different dopants, Mater. Sci. Technol. 24 (2008) 589–595.
[14] G. Grubert, M. Stockenhuber, O.P. Tkachenko, M. Wark, Titanium oxide species in molecular sieves: materials for the optical sensing of reductive gas atmospheres, Chem. Mater. 14 (2002) 2458–2466.
[15] R. Chatti, S.S. Rayalu, N. Dubey, N. Labhsetwar, S. Devotta, Solar-based photoreduction of methyl orange using zeolite supported photocatalytic materials, Sol. Energy Mater. Sol. Cells 91 (2007) 180–190.
[16] M. Alvaro, E. Carbonell, H. García, Photocatalytic degradation of sulphur-containing aromatic compounds in the presence of zeolite-bound 2,4,6-triphenylpyrylium and 2,4,6-triphenylthiapyrylium, Appl. Catal. B 51 (2004) 195–202.
[17] W. Panpa, P. Sujaridworakun, S. Jinawath, Photocatalytic activity of TiO_2/ZSM-5 composites in the presence of SO_4^{2-} ion, Appl. Catal. B 80 (2008) 271–276.
[18] M. Huang, C. Xu, Z. Wu, Y. Huang, J. Lin, J. Wu, Photocatalytic discolorization of methyl orange solution by Pt modified TiO_2 loaded on natural zeolita, Dyes Pigments 77 (2008) 327–334.
[19] C. Aprile, A. Corma, H. Garcia, Enhancement of the photocatalytic activity of TiO_2 through spatial structuring and particle size control: from subnanometric to submillimetric length scale, Phys. Chem. Chem. Phys. 10 (2008) 769–783.
[20] S. Anandan, Photocatalytic effects of titania supported nanoporous MCM-41 on degradation of methyl orange in the presence of electron acceptors, Dyes Pigments 76 (2008) 535–541.
[21] D.I. Petkowicz, R.T. Rigo, C. Radtke, S.B.C. Pergher, J.H.Z. dos Santos, Zeolite NaA from Brazilian chrysotile and rice husk, Micropor. Mesopor. Mater. 116 (2008) 548–554.
[22] J. Liqianga, S. Xiaojuna, C. Weimina, X. Zilic, D. Yaoguoc, F. Honggang, The preparation and characterization of nanoparticle TiO_2/Ti films and their photocatalytic activity, J. Phys. Chem. Solids 64 (2003) 615–623.
[23] D.I. Petkowicz, R. Brambilla, C. Radtke, C.D.S. da Silva, Z.N. da Rocha, S.B.C. Pergher, J.H.Z. dos Santos, Photodegradation of blue methylene by in situ generated titania supported on NaA zeolite, Appl. Catal. A: Gen. 357 (2009) 125–134.
[24] W. Cheng-Cai, L. Chung-Kung, L. Meng-Du, J. Lain-Chuen, Photocatalytic degradation of C.I. Basic Violet 10 using TiO_2 catalysts supported by Y zeolite: an investigation of the effects of operational parameters, Dyes Pigments 76 (2008) 817–824.
[25] M. Huang, C. Xu, Z. Wu, Y. Huang, J. Lin, J. Wu, Photocatalytic discolorization of methyl orange solution by Pt modified TiO_2 loaded on natural zeolite, Dyes Pigments 77 (2008) 327–334.
[26] M.A. Aramendía, J.C. Colmenares, S. López-Fernández, A. Marinas, J.M. Marinas, F.J. Urbano, Screening of different zeolite-based catalysts for gas-phase selective photooxidation of propan-2-ol, Catal. Today 129 (2007) 102–109.
[27] C.B. Khouw, C.B. Dartt, J.A. Labinger, M.E. Davis, Studies on the catalytic oxidation of alkanes and alkenes by titanium silicates, J. Catal. 149 (1994) 195–205.
[28] A.J.H.P. van der Pol, A.J. Verduyn, J.H.C. van Hooff, Why are some titanium silicalite-1 samples active and others not? Appl. Catal. A 92 (1992) 113–130.
[29] R.J. Davis, Z. Liu, J.E. Tabora, W.S. Wielband, X-ray absorption spectroscopy of Ti-containing molecular sieves ETS-10, aluminum-free Ti-β, and TS-1, Catal. Lett. 34 (1995) 101–113.
[30] F. Geobaldo, S. Bordiga, A. Zecchina, E. Giamello, G. Leofanti, G. Petrini, DRS UV–Vis and EPR spectroscopy of hydroperoxo and superoxo complexes in titanium silicalite, Catal. Lett. 16 (1992) 109–115.
[31] N. Phonthammachai, M. Krissanasaeranee, E. Gulari, A.M. Jamieson, S. Wongkasemjit, Crystallization and catalytic activity of high titanium loaded TS-1 zeolite, Mater. Chem. Phys. 97 (2006) 458–467.
[32] M. Koelsch, S. Cassaignon, C.T.T. Minh, J.F. Guillemoles, J.P. Jolivet, Electrochemical comparative study of titania (anatase, brookite and rutile) nanoparticles synthesized in aqueous medium, Thin Solid Films 451 (2004) 86–92.
[33] P. Jantawasu, T. Sreethawong, S. Chavadej, Photocatalytic activity of nanocrystalline mesoporous-assembled TiO_2 photocatalyst for degradation of methyl orange monoazo dye in aqueous wastewater, Chem. Eng. J. 155 (2009) 223.
[34] X. Du, E. Wu, Porosity of microporous zeolites A, X and ZSM-5 studied by small angle X-ray scattering and nitrogen adsorption, J. Phys. Chem. Solids 68 (2007) 1692–1699.
[35] J. Saien, A.R. Soleymani, Degradation and mineralization of Direct Blue 71 in a circulating up flow reactor by UV/TiO_2 process and employing a new method in kinetic study, J. Hazard. Mater. 144 (2007) 506–512.
[36] S.A. Kumar, P.-H. Lo, S.-M. Chen, Electrochemical selective determination of ascorbic acid redox active polymer modified electrode derived from direct blue 71, Biosens. Bioelectron. 24 (2008) 518–523.
[37] M. Bekbölet, M. Lindner, D. Weichgrebe, D.W. Bahnemann, Photocatalytic detoxification with the Thin-Film Fixed-Bed Reactor (TFFBR): clean-up of highly polluted landfill effluents using a novel TiO_2-photocatalyst, Sol. Energy 56 (1996) 455–469.
[38] E. Selli, D. Baglio, L. Montanarella, G. Bidoglio, Role of humic acids in the TiO_2-photocatalyzed degradation of tetrachloroethene in water, Water Res. 33 (1999) 1827–1836.